Journal of
Materials Chemistry A

Accepted Manuscript

Volume 4 | Number 1 | 7 January 2016 | Pages 1–330

Journal of
Materials Chemistry A

Materials for energy and sustainability
www.rsc.org/MaterialsA

ISSN 2050-7488

ROYAL SOCIETY OF CHEMISTRY

PAPER
Kun Chang, Zhaorong Chang et al.
Bubble-template-assisted synthesis of hollow fullerene-like
MoS₂ nanocages as a lithium ion battery anode material

175 YEARS

This is an Accepted Manuscript, which has been through the Royal Society of Chemistry peer review process and has been accepted for publication.

Accepted Manuscripts are published online shortly after acceptance, before technical editing, formatting and proof reading. Using this free service, authors can make their results available to the community, in citable form, before we publish the edited article. We will replace this Accepted Manuscript with the edited and formatted Advance Article as soon as it is available.

You can find more information about Accepted Manuscripts in the author guidelines.

Please note that technical editing may introduce minor changes to the text and/or graphics, which may alter content. The journal's standard Terms & Conditions and the ethical guidelines, outlined in our author and reviewer resource centre, still apply. In no event shall the Royal Society of Chemistry be held responsible for any errors or omissions in this Accepted Manuscript or any consequences arising from the use of any information it contains.

ROYAL SOCIETY OF CHEMISTRY

rsc.li/materials-a

Journal Name

ARTICLE

New Anatase Phase $VTi_{2.6}O_{7.2}$ Ultrafine Nanocrystals for High-Performance Rechargeable Magnesium-Based Batteries†

Jinzhi Sheng,‡[a] Chen Peng,‡[a] Siwen Yan,‡[a] Guobin Zhang,[a] Yalong Jiang,[a] Qinyou An,*[a] Qiulong Wei,[ab] Qiang Ru,[c] and Liqiang Mai*[a]

Magnesium-based batteries are regarded as a potential candidate of the next-generation energy storage devices due to their safety and low cost. However, the existing cathode materials still suffer from slow ions diffusion kinetics and relatively inferior electrochemical performance. In this work, we design and synthesize a kind of new anatase phase $VTi_{2.6}O_{7.2}$ ultrafine nanocrystals (VTO) with fast intercalation kinetics. As a cathode material for magnesium batteries (MBs), VTO exhibits the capacity of 121.9 mAh g^{-1} at 20 mA g^{-1}. When applied to magnesium-lithium hybrid batteries (MLHBs), VTO exhibits high specific capacity (265.2 mAh g^{-1} at 50 mA g^{-1}), good cycling stability (84.2% capacity retention after 1200 cycles) and high rate capability (64.9 mAh g^{-1} at 2 A g^{-1}). The good performances are attributed to the enhanced diffusion kinetics, increased cations storage active sites and shortened ion diffusion path. Furthermore, the lithium storage mechanism in VTO was studied via the in situ XRD measurement. These results demonstrate that VTO is a promising electrode material for magnesium-based batteries, and constructing substitutional solid solution is an effective way to exploit and optimize new types of electrode materials with enhanced performances.

Introduction

In order to alleviate the increasing serious energy crisis and meet the rapidly growing industrial development needs, environmentally friendly energy storage systems are demanded to provide higher energy density, improved security and longer service life.[1-2] As a typical kind of energy storage device, lithium ion batteries (LIBs) have dominated the portable electronic products market in the past few decades because of their relatively high energy density and long cycle life.[3-4] However, they may hardly be further developed owing to the inhibition of the growing price of lithium resources and the unsatisfied capacity of graphite anode (372 mAh g^{-1}).[5] In addition, the development of lithium batteries (LBs) are limited by the hidden danger of lithium dendrite growth, even though the theoretical capacity of lithium metal reaches 3862 mAh g^{-1}.[3,5] Comparatively speaking, rechargeable magnesium batteries (MBs) recently have received significant attention due to its safety (no dendrites growth). The higher volumetric energy density of Mg (3833 mAh cm^{-3} vs. 2061 mAh cm^{-3} of Li)

and its lower price also make MBs become the candidate of the next generation energy storage system.[6-7] However, the slow kinetics of Mg^{2+} intercalation in the cathode host is a major obstacle to the development of MBs.[6,8-9] Thus, exploring suitable cathode materials with fast ion intercalation kinetics is one of the most important directions to be headed for MBs.

As a widely investigated electrode material for LIBs, anatase TiO_2 shows stable discharge voltage plateau (~1.7 V vs. Li+/Li), long cycling stability and excellent rate performance.[10-12] However, the results are not satisfactory when it was applied in MBs due to the sluggish diffusion kinetics of Mg^{2+} in TiO_2. The magnesium-lithium hybrid batteries (MLHBs) system combines the high capacity of magnesium metal anode and the rapid Li+ diffusion kinetics of cathode materials, solving both the main defects of LIBs and MBs in a certain extent. As cathode materials in MLHBs, Su et al. and Meng et al. reported that the TiO_2 shows 115 mAh g^{-1} at 670 mA g^{-1} with the discharged voltage plateau of ~0.7 V within 200 cycles, and 114 mAh g^{-1} at 1.0 A g^{-1} with the voltage plateau of ~0.65 V, respectively.[13-14] Compared to other reported cathode materials (VO_2[15], TiS_2[16-17], FeS_x (x = 1 or 2)[18]) of MLHBs, although the stable anatase structure of TiO_2 is advantageous, its low rate capacity and average discharge voltage still need to be further solved. Constructing substitutional solid solution is effective to optimize the electrochemical performances via adjusting interatomic interaction, which have been proved more than once in previous researchers, such as $LiNi_{0.5}Mn_{1.5}O_4$[19], $Li(Ni_{1/3}Co_{1/3}Mn_{1/3})O_2$[20] and $Li(Ni_{0.5}Co_{0.2}Mn_{0.3})O_2$[21]. Vanadium, as one of the few elements with high electrochemical activity[22-24], is just next to titanium

[a] State Key Laboratory of Advanced Technology for Materials Synthesis and Processing, International School of Materials Science and Engineering, Wuhan University of Technology, Luoshi Road 122, Wuhan, 430070, P. R. China.
 *E-mail: anqinyou86@whut.edu.cn (Q. An); mlq518@whut.edu.cn (L. Mai).
[b] Department of Chemistry, University of California, Berkeley, CA 94720, USA.
[c] Guangdong Engineering Technology Research Center of Efficient Green Energy and Environmental Protection Materials, South China Normal University, Guangzhou 510006, P. R. China.
‡ These authors contributed equally to this work.
† Electronic Supplementary Information (ESI) available.

ARTICLE

in the same transition-metal of the 4th period, which is appropriate to form substitutional solid solution with titanium due to their very similar atomic radius and electronegativity.[25] In addition, according to the calculations of density functional theory (DFT), when V atoms replace some Ti atoms in TiO_2 crystal lattice, both the intercalation energy and volume expansion significantly decreases after the intercalation of Li^+, which suggests the possibility of the optimized battery performance (**Fig. S1** and **Table S1**). Therefore, combining the high electrochemical activity of vanadium and the structural stability of titanium, a new cathode material with high discharge voltage, high capacity and long cycling life for MLHBs could be probably designed and constructed.

Herein, for the first time, we report a kind of new anatase phase $VTi_{2.6}O_{7.2}$ ultrafine nanocrystals (VTO) designed via constructing the ingenious substitutional solid solution. As the cathode material for MBs, VTO shows a relatively high capacity of 121.9 mAh g^{-1} at 20 mA g^{-1}. When applied to MLHBs, it exhibits high capacity of 265.2 mAh g^{-1} (coin-type batteries), high rate capability of 64.9 mAh g^{-1} at 2 A g^{-1} and good cycling stability of 84.2% capacity retention after 1200 cycles. The good results are attributed to the enhanced diffusion kinetics, increased cations storage active sites and shortened ion diffusion path. Furthermore, the lithium storage mechanism in $VTi_{2.6}O_{7.2}$ was further studied by in situ XRD, and the Mg^{2+}/Li^+ co-intercalation reaction in MLHBs are proved by electrochemical measurements.

Experimental Section

Sample Preparation

To obtain the anatase $VTi_{2.6}O_{7.2}$ (noted as VTO), 2 mmol $V(IV)O(acac)_2$ blue-green crystal and 2 mmol $K_2TiO(C_2O_4)$ white crystalline powder are dissolved in 80 mL deionized water by stirring violently for about 30 min. Then, the acquired transparent and homogeneous green solution is transferred into 100 mL Teflon-lined autoclave followed by heating at 200 °C for about 10 h. Next, after natural cooling to room temperature and several washing with deionized water and alcohol, blackish green precipitation can be collected. It must be noted that the precipitation must be dried at 60 °C in vacuum to obtain the final dark green product.

Materials Characterization

X-ray diffraction (XRD) results were obtained by the Bruker D8 Advance X-ray diffractometer with a Cu Ka X-ray source) conducted employed to characterize the crystallographic information. Raman spectra were obtained using a Renishaw INVIA micro-Raman spectroscopy system. Scanning electron microscope (SEM) images and energy dispersive spectrometer (EDS) were collected with a JEOL-7100F SEM/EDS microscope. Transmission electron microscope (TEM) images were recorded by using a JEM-2100F STEM/EDS microscope. Brunauer-Emmett-Teller (BET) surface areas were measured using a Tristar II 3020 instrument by adsorption of nitrogen at

77 K. X-ray photoelectron spectroscopy (XPS) measurement was performed using a VG Multi Lab 2000 instrument.

Measurements of Electrochemical Performances

The electrochemical properties were measured by assembly of 2016 coin cells in a glove box filled with pure argon gas. In MBs and MLHBs with Mg foil as the anode, the All-phenyl complex (APC) and APC-LiCl (1 M LiCl in 0.25 M APC) electrolytes were prepared on the basis of the reported method, respectively. In lithium and sodium half cells with Li and Na metal was used as the anode, 1 M solution of $LiClO_4/NaClO_4$ in ethylene carbon (EC)–dimethyl carbonate (DMC) (1:1 w/w) with 5% FEC were used as the electrolyte, and a whatman glass fiber (GF/D) was used as the separator. The electrodes were fabricated to form a freestanding film with a weight ratio of 60% $VTi_{2.6}O_{7.2}$ active material, 30% acetylene black and 10% PTFE using a roller mill and dried in an oven over 12 h at 70 °C. The mass loading was approximately 5.0-10.0 mg cm^{-2}. Galvanostatic charge–discharge measurement was tested by a multi-channel battery testing system (LAND CT2001A). Voltammetry (CV) curves and electrochemical impedance spectra (EIS) were carried out at an Autolab PGSTAT 302 electrochemical workstation.
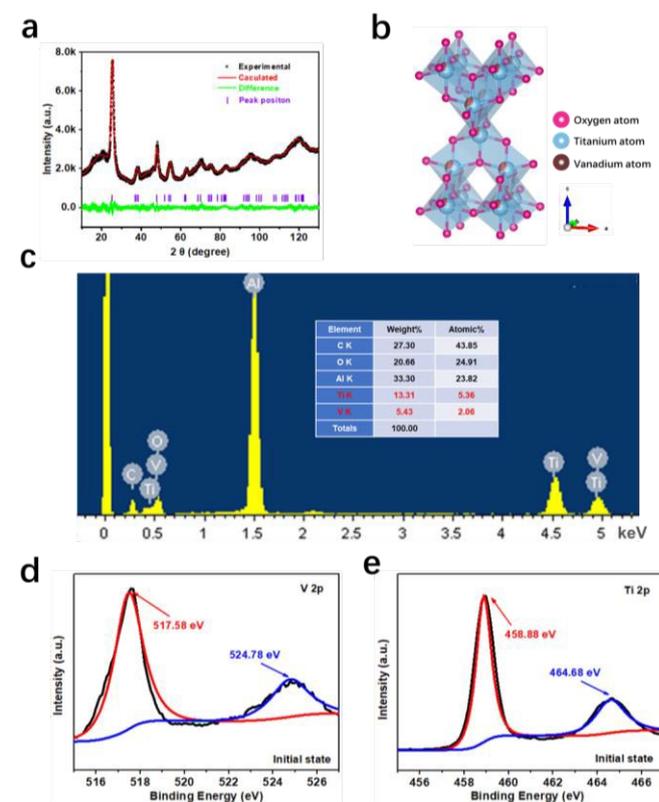
Results and Discussions

Fig. 1 Crystal structure and element composition of VTO. (a) The Rietveld plot for refined $VTi_{2.6}O_{7.2}$ XRD pattern with experimental data in black dots, calculated curve in red, difference curve in green and short vertical line in purple. (b) Crystal structure. (c) EDS microanalysis. (d, e) XPS spectra of V 2p and Ti 2p in the initial state.

To analyze the crystal structure of VTO, the Rietveld refined XRD pattern of VTO is shown, in which the major diffraction peaks matched well with the calculated pattern, suggesting the pure phase of $VTi_{2.6}O_{7.2}$ (**Fig. 1a**). The refined crystal structure (**Fig. 1b**) shows an anatase structure, which belongs to tetragonal system with cell parameters of a=b=3.80 Å and c=9.51 Å. After Ti atoms are partially substituted by V atoms, the TiO_6 octahedron distorted and the cell parameters increased compared with the standard anatase TiO_2 (JCPDS NO. 01-073-1764), indicating the larger lattice spacing for ions storage.[26] More detailed calculations are shown in **Table S2** and **S3**. To further verify the interaction between Ti, V and O atoms, Raman spectroscopy is carried out (**Fig. S2**). The characteristic peaks located at 393, 506, 625 cm^{-1} match well with the anatase phase, corresponding to the O-Ti-O symmetric bending vibration (B_{1g} modes), O-Ti-O antisymmetric bending vibration (A_{1g} modes) and O-Ti-O symmetric stretching vibration (E_g modes), respectively.[27-28] And the bands at 150 and 186 cm^{-1} are very close to that in vanadium oxide, associated with the lattice vibration (external modes)[29-30], suggesting the strong chemical bond (not weak Van der Waal's force) between the V atoms and the O atoms in the crystal structure. The EDS result shows that the atomic ratio of V: Ti is 1:2.60 (**Fig. 1c**), which is coincide to the result of 1:2.67 obtained by the inductively coupled plasma (ICP) measurement. XPS measurement is carried out to confirm the primary valence states of V and Ti for the final chemical formula of this new anatase material. In the V 2p core-level spectrum (**Fig. 1d**), the peaks at 517.58 and 524.78 eV are associated with $2p_{3/2}$ and $2p_{1/2}$ of V^{4+}, respectively.[31-32] In the Ti 2p core-level spectrum (**Fig. 1e**), the peaks at 458.88 and 464.68 eV corresponds to $2p_{3/2}$ and $2p_{1/2}$ of Ti^{4+},

respectively.[33-34] According to the results of EDS, ICP and XPS, the chemical formula that $VTi_{2.6}O_{7.2}$ can be confirmed for the law of conservation of charge.

The morphology and microstructure of $VT_{2.6}O_{7.2}$ is characterized by the SEM and TEM. **Fig. 2a** and **2b** show that the product consists of micron bulks packed tightly by many dendritic-like nanoparticles with rough surface and numberous small holes. The BET measurement dispalys that its surface area reaches 156.7 m^2 g^{-1}, and the broad peak in the inset of **Fig. 2f** suggests that the size of pores distributes in 2-20 nm formed via nanoparticles stacking.[35] In **Fig. 2c**, many roe-like solid nanopaticles on the surface of dendritic-like short nanorods are distributed with different density in different regions, of which the boundary is clear, and the ultrafine nanocrystals of ~10 nm diameter are observed (**Fig. 2d**). In high revolution TEM (**Fig. 2e**), two obvious lattice fringes with interplanar distances of 3.53 and 2.43 Å are indexed with the lattice plane (011) and (013), respectively. To further observe the elements distribution of the substitutional solid solution, EDS-mapping was carried out, and the result shows that Ti, V and O are uniformly distrubed in the sample (**Fig. 2g**).

Coin-type batteries were assembled to investigate the electrochemical performances of VTO. As cathode material in MBs, under the voltage range of 0.01–1.9 V (vs. Mg^{2+}/Mg) and the scan rate of 0.1 mV s^{-1}, no obvious peaks are observed (**Fig. 3a**), in agreement with the charge–discharge curves shown in **Fig. 3b**. Because the particle size of the VTO sample is very small and the specific surface area is large, the Mg storage capacity tends to be contributed by the Faradaic pseudocapacitance charge storage on the surface instead of diffusion-controlled intercalation.[36-37] The pseudocapacitance charge storage process may not lead to the same changing of the Gibbs free energy, so the plateau is not exhibited obviously.[38] Under the current density of 100 mA g^{-1}, it exhibits the initial discharge capacity of 195.8 mAh g^{-1}, and 103.9 mAh g^{-1} remains in the second cycle. The irreversible capacity loss is caused by the formation of the solid electrolyte interphase (SEI). Under the relatively low voltage range, the magnesium metal anode corrodes in the $A1Cl_3$-$MgCl_2$ solution, forming a passivating layer consisted of some insoluble products of the reaction of the metal with the solution.[39] This process will provide a certain charge transfer, which reflects as the irreversible capacity. After 100 cycles, the reversible capacity of 56.3 mAh g^{-1} with amost 100% coulombic effciency is still obtained (**Fig. 3c**), which is much better than the reported TiO_2.[13,14] The relatively high discharge capacity of 121.9 mAh g^{-1} at 20 mA g^{-1} is obtained, and at 500 mA g^{-1}, the capacity remains 29.4 mAh g^{-1} (**Fig. 3d**). After the current density reverted to 20 mA g^{-1}, the capacity of 72.3 mAh g^{-1} is still attained. The maximum value of intercalating Mg^{2+} can be estimated at 0.68 per formula unit with **Equation S1** according to the largest reversible capacity of 121.9 mAh g^{-1}. For comparison, the pure phase anatase TiO_2 synthesized via the
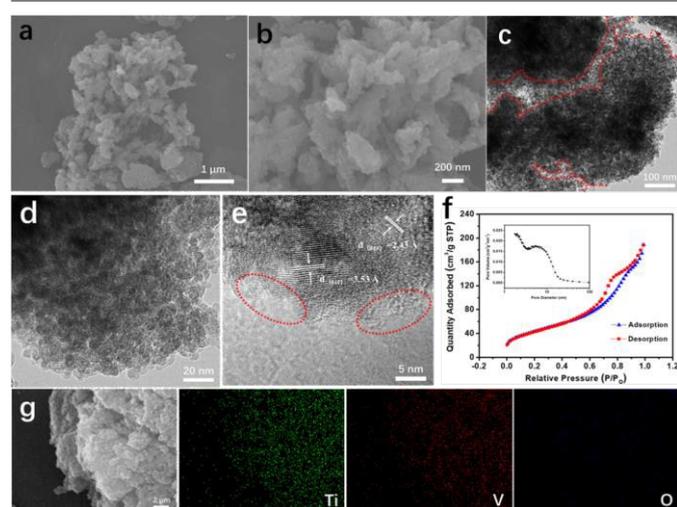

Fig. 2 Morphology and microstructure of VTO. (a) Low-magnification SEM images. (b) High-magnification SEM images. (c) TEM images. Red dotted line, the boundry between two regions of different density. (d) TEM images. (e) HRTEM images. Red dotted ellipse, amorphous region. (f) Nitrogen adsorption and desorption isotherms and pore size distribution (Inset). (g) EDS-mapping of large-scale area.
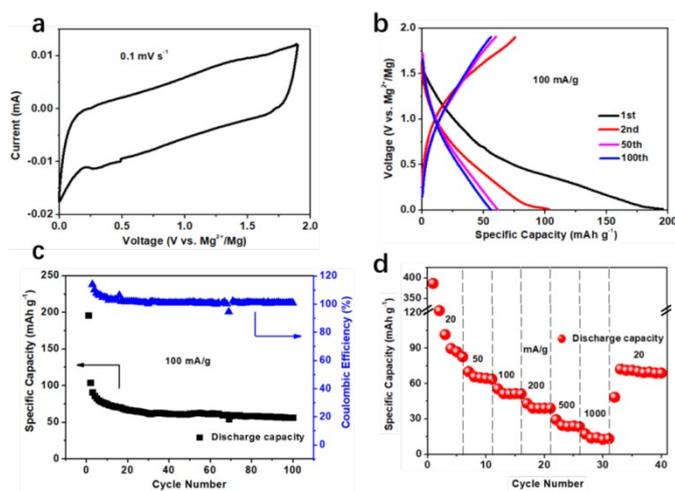
Fig. 3 Electrochemical performance of VTO in MBs. (a) Cyclic voltammogram curve (scan rate, 0.1 mV s^{-1}). (b) Charge-discharge curves of different cycles at 100 mA g^{-1} in the voltage window of 0.01-1.9 V. (c) Cycling performance at 100 mA g^{-1}. (d) Rate performances.

same method of VTi$_{2.6}$O$_{7.2}$ without adding V(IV)O(acac)$_2$ is fabricated. The refined XRD pattern and the crystal parameters are given in **Fig. S3a**, **Table S4** and **Table S5**. The XRD results and SEM image (**Fig. S3b**) show that the crystal structure and morphology of TiO$_2$ is very similar with that of VTi$_{2.6}$O$_{7.2}$. When applied in MBs, the sample exhibits the capacity of 18 mAh g^{-1} in the first cycle, and almost no capacity from the second cycle, which indicates that introducing vanadium into TiO$_2$ is effective to improve the magnesium storage performance (**Fig. S4**). To investigate the magnesium storage mechanism, ex situ XRD measurement was taken out (**Fig. S5**). During the first discharge and charge process, the diffraction peaks belonged to VTi$_{2.6}$O$_{7.2}$ show no significant change, indicating that the anatase crystal structure does not change during Mg ions storage. This result precludes the possibility of conversion reaction or alloying reaction. Bases on the previous electrochemical measurement results, the Mg ions storage reaction tends to be the Faradaic pseudocapacitance charge storage.

In order to investgate the ability of lithium storage, LIBs were assembled. **Fig. S6a** shows the cyclic voltammogram curve at the scan rate of 0.1 mV s^{-1}. The cathodic/anodic peaks at 1.84/2.19 V are consistent with the Li$^+$ ion incalatation/deincalatation[11,12], correspongding to the plateaus in the charge-discharge curves (**Fig. S6b**). The rate performance is shown in **Fig. S6c**, and the a high-rate capacity of 113.8 mAh g^{-1} is obtained even at 10 A g^{-1}, demonstrating the fast diffusion kenetic of Li$^+$ ions in VTO host. Furthermore,
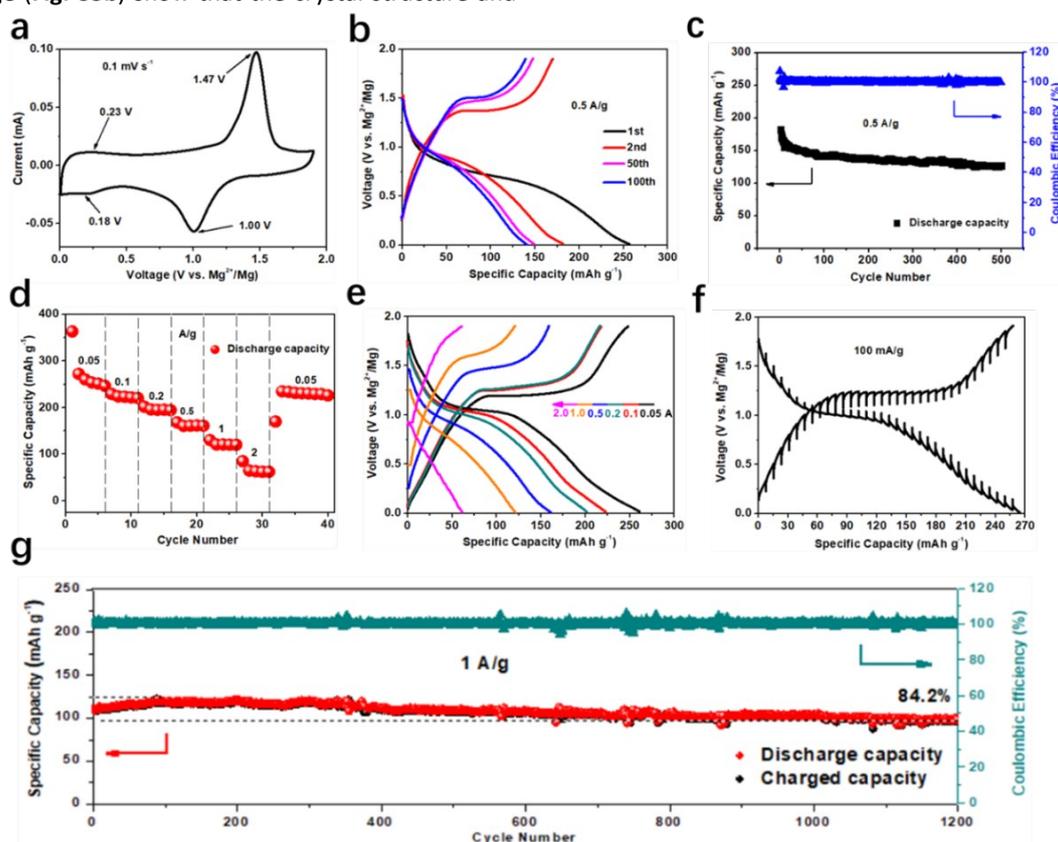

Fig. 4 Electrochemical performance of VTO in MLHBs. (a) Cyclic voltammogram curve (scan rate, 0.1 mV s^{-1}). (b) Charge-discharge curves of different cycles at 0.5 A g^{-1} in the voltage window of 0.01-1.9 V. (c) Cycling performance at 0.5 A g^{-1}. (d) Rate performances. (e) Charge-discharge curves at different rates. (f) GITT curves of VTO in the second cycle. (g) Long cycling performance at 1 A g^{-1}.

ARTICLE

this new anatase material can also storage Na^{+} and good performances are obtained (**Fig. S7**). The above results demonstrate its versatile application in different secondary battery systems.

Daniell-type batteries can effectively improve the specific energy density by adding Li salt into the electrolyte of MBs, which combine the advantages of high specific capacity, fast diffusion kinetics of Li^{+} and no dentrite growth in MBs.[40-41] Inspired by this concept, we assembled the MLHBs with VTO as cathode, Mg metal as anode and APC-LiCl mixture as eletrolyte. Comparing with the cathodic/anodic peaks at 1.00/1.47 V of MLHBs and 1.84/2.19 V of LIBs in CV curves (**Fig. 4a, S5a**), the Li^{+} ions are likely to intercalate/deintercalate in the host in this process due to the~0.7 V higher potential of Mg^{2+}/Mg than Li^{+}/Li.[6,8] Combining the previous results in MBs, it may suggested a co-intercalation reaction of Mg^{2+} and Li^{+}.[42] The charge-discharge curves in different cycles at 500 mA g^{-1} and its corresponding cycling performance are shown in **Fig. 4b** and **4c**. The charge and discharge plateau is about 1.50 V and 0.85 V, respectively. The capaity of 182.7 mAh g^{-1} is obtained under the current density of 0.5 A g^{-1}, and still maintained 126.1 mAh g^{-1} after 500 cycles. The theoretical capacity of $VTi_{2.6}O_{7.2}$ is calculated according to Equation S1 based on the complete valence states changing that all the V[4+] and Ti^{4+} change into V[3+] and Ti^{3+}, respectively. This result corresponds to 3.6 charge transfer, which will provide the theoretical capacity of 331.6 mAh g^{-1}. The initial discharge capacity reaches to 363.4 mAh g^{-1} at the current destiny of 0.05 A g^{-1}. The extra capacity beyond the theoretical capacity may be contributed by the capacitive charge storage.[43] Even at 2.0 A g^{-1}, it still delivers 64.9 mAh g^{-1} (**Fig. 4d, 4e**), wihch is better than reported TiO_2.[14,15] Under the high current density, the Faradaic pseudocapacitance capacitive charge storage will account for a significant proportion instead of the diffusion-controlled intercalation contribution.[36-37] The pseudocapacitance charge storage process may not lead to the same changing of the Gibbs free energy, so the plateau is not exhibited obviously.[38] Galvanostatic intermittent titration technique (GITT) curves in the second cycle at 0.1 A g^{-1} displays that the actual maximum value of spcificic discharge capacity is 265.2 mAh g^{-1} (**Fig. 4f**), meaning that the specific energy density is about 265.2 Wh kg^{-1} (the average discharge voltage is estimated at around 1.0 V). The long cycling performance at high current density of 1 A g^{-1} was shown in **Fig. 4g**. The capacity of 122.2 mAh g^{-1} is obtained with 84.2% retention after 1200 cycles, exhibitng an excellent cycling stablity. The as prepared TiO_2 sample is also tested as the cathode in MLHBs (**Fig. S8**). When cycling under the current density of 100 mA g^{-1}, it shows the reversible capacity of ~120 mAh g^{-1}. After 200 cycles, the capacity decreases obviously to less than 20 mAh g^{-1}. The result confirms the positive effect of constructing substitutional solid solution.

Because of the limits of the immature technoogy (the stainless steel electrode shell will accelerate the decomposition of APC electrolytes during the measurement) of in situ XRD in rechareable MBs, the Li^{+} storage mechanism

of VTO as the cathode in LIB was investigated instead. **Fig. 5a** shows both the charge-discharge curves of VTO in the first/second cycles under the voltage window of 0.01-3.5 V at the current density of 0.5 A g^{-1} and the corresponding 2D in situ XRD pattern. When the coin cell was discharged to ~1.75 V in the first cycle, the peak at ~25° associated with the (101) lattice plane shifts to a lower angle, indicating the increased lattice spacing, which is ascribed to the selective inserting of Li^{+} to these lattice planes.[43] During the discharge process from 1.75 V to 0.01 V in the first cycle and the charge process from 0.01 V to 2.00 V in the second cycle, no obvious change is observed. When charged from 2.00 V to 3.5 V, the peak at ~25° shifts back to the higher angle, because of the reversible lattice distortion caused by the excessive extraction of Li^{+}.[44] Because the other peaks of VTO are too weak to be observed under the strong peaks of Be and BeO, so we only display the peak of VTO at ~25° in the in situ XRD pattern. To further study the mechanism of Mg^{2+}/Li^{+} co-intercalation in MLHBs, XPS measuraments are carried out to confirm the valence state
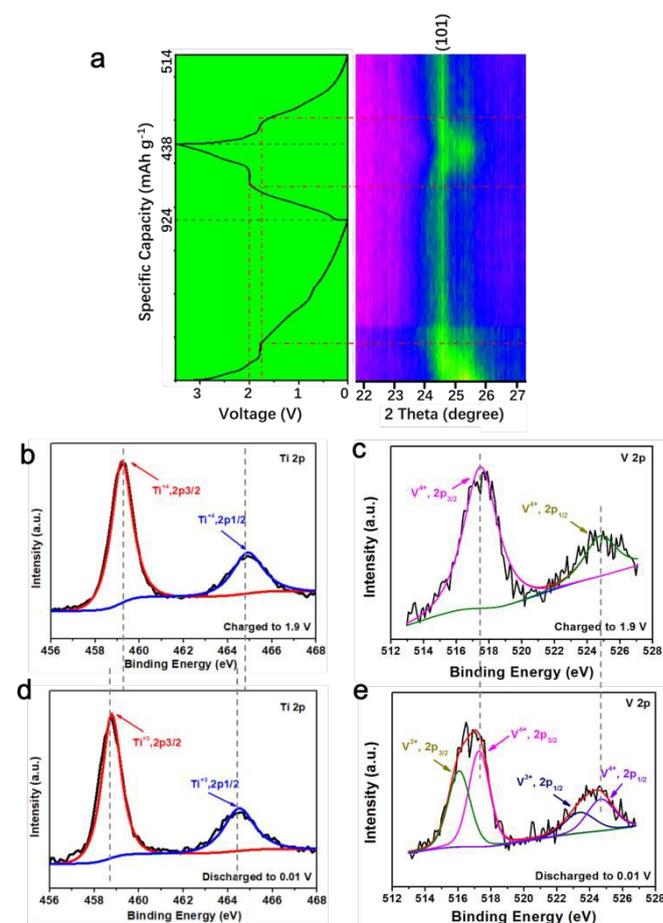

Fig. 5 Mechanism of ions storage in VTO. (a) In situ XRD measurement in LIBs. (b, c) XPS spectra of Ti 2p and V 2p after the sample was charged to 1.9 V in MLHBs. (d, e) XPS spectra of Ti 2p and V 2p after the sample was discharged to 0.01 V in MLHBs.
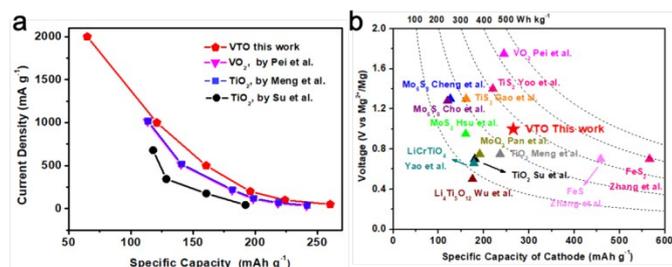
Fig. 6 Comparison in coin-type MLHBs electrochemical performances. (a) Comparison of the reported TiO_2, VO_2 and this work in electrochemical performance. (b) Comparison of the reported different cathode materials and this work in specific energy density.

changes of Ti and V elements. When charged to 1.9 V, the peaks at 459.27 and 464.87 eV are associated with $2p_{3/2}$ and $2p_{1/2}$ of Ti^{4+}, respectively (**Fig. 5b**).[45-46] After discharged to 0.01 V, these two peaks shifted to lower bondingnergy located at 458.78 and 464.48 eV, corresponding to the Ti^{3+} (**Fig. 5d**)[47-48], indicating the 2.6 charge transfer per formula unit. When charged to 1.9 V, the peaks for V $2p_{3/2}$ and $2p_{1/2}$ were observed at 517.47 and 524.77 eV, respectively, corresponding to the V^{4+} (**Fig. 5c**).[31-32] After discharged to 0.01 V, after fitting, the V $2p_{3/2}$ spectrum can be deconvoluted into two peaks located at 515.98 and 517.18 eV, which belong to V^{3+} and V^{4+}, respectively.[31,49] And the V $2p_{1/2}$ spectrum can also be deconvoluted into two peaks located at 523.48 and 524.68 eV, which are associated to V^{3+} and V^{4+}, respectively (**Fig. 5e**).[32,50] In addtion, the peak areas of V^{3+} and V^{4+} are closed to ~1:1, suggesting that almost 50% of V^{4+} were reduced to V^{3+}, which is corresponded to ~0.5 charge transfer. These result are consistent with the actual maximum value of spcificic discharge capacity of 265.2 mAh g^{-1} with about 3 charge transfer (if calculated based on the theoretical capacity, it will be more than 3 charge transfer) per formula unit. Obviously, the redox pair of Ti^{4+}/Ti^{3+} and V^{4+}/V^{3+} are both highly reversible[10-11, 22-23], which explained the good cycling stability of VTO.

In order to intuitively reflect the advantages of $VT_{2.6}O_{7.2}$ in rechargable MLHBs, comparison of typical cathode materials in coin-type MLHBs performances are displayed. As shown in **Fig. 6a**, VTO exhibits higher rate capacity than both VO_2[15] and TiO_2[13-14], especially in high current density. Besides, the capacity of 98.4 mAh g^{-1} at 1 A g^{-1} with 1200 cycles is obtained, which is much better than VO_2 in cycle life. In addition, the dischage voltage of ~1 V is also 0.2 V higher than TiO_2. Moreover, in MBs, VO_2 and TiO_2 basically do not provide much reversible capacity except TiO_2 reported by Meng et al[14]. On the contrary, VTO shows a high reversible capacity of 121.9 mAh g^{-1} in MBs. The specific energy density calculated based on the mass of different cathode materials in coin-type MLHBs was displayed in **Fig. 6b**. Compared to other reported cathode materials of TiO_2[13-14], $Li_4Ti_5O_{12}$[39], Mo_6S_8[51-52], MoS_2[53], MoO_2[54], $LiCrTiO_4$[55] (at low current density, not more than 100 mA g^{-1}), VTO delivers higher discharged capacity of 265.2 mAh g^{-1}, which demonstrates its great potential in magnesium-based

batteries. The detailed experiment parameters of these works are listed in **Table S6**.

After comparing the different important indexes in battery field , it is apparent that VTO exhibits higher specific capacity, higher voltage than TiO_2 and higher cycling stability than VO_2. The improved electrochemical performances owe to the successful V substitution design. Firstly, after V occupied part of the sites of Ti, the new phase preserves the stable anatase structure of TiO_2, which is beneficial to longer cycle life. Secondly, with the accession of V, the transferable charge in the material increases substantially, resulting in higher reversible capacity. Thirdly, the lattice spacing is expanded after V substitution, which will provide larger ion diffusion channel. These results prove that constructing substitutional solid solution is effective to optimize the electrochemical performances.

Conclusions

In summary, we designed a new type anatase $VTi_{2.6}O_{7.2}$ ultrafine nanocrystals with fast intercalation kinetics via constructing substitutional solid solution. As the cathode material for the MBs, a reversible capacity of 121.9 mAh g^{-1} was obtained. When applied to MLHBs, it exhibited high capacity of 265.2 mAh g^{-1}, high rate capability of 64.9 mAh g^{-1} at 2 A g^{-1} and good high-rate cycling stability with 84.2% capacity retention after 1200 cycles at 1 A g^{-1}. The good electrochemical performances are attributed to the fast intercalation kinetics in VTO host. Furthermore, the mechanism of lithium storage was thoroughly studied by in situ XRD. Our work paves the way for the original design of new type phase cathode materials from the atoms level and various effective research ideas in rechargeable batteries of Mg system.

Conflicts of interest

There are no conflicts to declare.

Acknowledgements

References

Journal Name

ARTICLE

1   M. Armand, J. M. Tarascon, *Nature*, 2008, **451**, 652.
2   B. Dunn, H. Kamath, J. M. Tarascon, *Science*, 2011, **334**, 928.
3   Z. Yang, J. Zhang, M. C. W. Kintner-Meyer, X. Lu, D. Choi, J. P. Lemmon, J. Liu, *Chem. Rev.*, 2011, **111**, 3577.
4   V. Etacheri, R. Marom, R. Elazari, G. Salitra, D. Aurbach, *Energy Environ. Sci.*, 2011, **4**, 3243.
5   P. Canepa, G. S. Gautam, D. C. Hannah, R. Malik, K. Liu, K. G. Gallagher, K. A. Persson, G. Ceder, *Chem. Rev.*, 2017, **117**, 4287.
6   D. Aurbach, Z. Lu, A. Schechter, Y. Gofer, H. Gizbar, R. Turgeman, Y. Cohen, M. Moshkovich, E. Levi, *Nature*, 2000, **407**, 724.
7   J. Sheng, C. Peng, Y. Xu, H. Lyu, X. Xu, Q. An, L. Mai, *Adv. Energy Mater.* 2017, **7**, 1700247.
8   I. Shterenberg, M. Salama, Y. Gofer, E. Levi, D. Aurbach, *Materials Research Society*, 2014, **39**, 453.
9   H. D. Yoo, I. Shterenberg, Y. Gofer, G. Gershinsky, N. Pour, D. Aurbach, *Energy Environ. Sci.*, 2013, **6**, 2265.
10 Y. Tang, Y. Zhang, J. Deng, J. Wei, H. L. Tam, B. K. Chandran, Z. Dong, Z. Chen, X. Chen, *Adv. Mater.*, 2014, **26**, 6111.
11 H. Ren, R. Yu, J. Wang, Q. Jin, M. Yang, D. Mao, D. Kisailus, H. Zhao, D. Wang, *Nano Lett.*, 2014, **14**, 6679.
12 H. Liu, W. Li, D. Shen, D. Zhao, G. Wang. *J. Am. Chem. Soc.*, 2015, **137**, 13161.
13 S. Su, Y. NuLi, Z. Huang, Q. Miao, J. Yang, J. Wang, *ACS Appl. Mater. Interfaces*, 2016, **8**, 7111.
14 Y. Meng, D. Wang, Y. Wei, K. Zhu, Y. Zhao, X. Bian, F. Du, B. Liu, Y. Gao, G. Chen, *J. Power Sources*, 2017, **346**, 134.
15 C. Pei, F. Xiong, J. Sheng, Y. Yin, S. Tan, D. Wang, C. Han, Q. An, L. Mai, *ACS Appl. Mater. Interfaces*, 2017, **9**, 17060.
16 T. Gao, F. Han, Y. Zhu, L. Suo, C. Luo, K. Xu, C. Wang, *Adv. Energy Mater.* 2014, **5**, 1401507.
17 H. D. Yoo, Y. Liang, Y. Li, Y. Yao, *ACS Appl. Mater. Interfaces*, 2015, **7**, 7001.
18 Y. Zhang, J. Xie, Y. Han, C. Li, *Adv. Funct. Mater.*, 2015, **25**, 7300.
19 X. Fang, M. Ge, J. Rong, C. Zhou, *ACS Nano*, 2014, **8**, 4876.
20 K.M. Shaju, G.V. Subba Rao, B.V.R. Chowdari, *Electrochimica Acta*, 2002, **48**, 145.
21 Z. Wu, X. Han, J. Zheng, Y. Wei, R. Qiao, F. Shen, J. Dai, L. Hu, K. Xu, Y. Lin, W. Yang, F. Pan, *Nano Lett.*, 2014, **14**, 4700.
22 L. Mai, L. Xu, C. Han, X. Xu, Y. Luo, S. Zhao, Y. Zhao, *Nano Lett.*, 2010, **10**, 4750.
23 S. Tepavcevic, H. Xiong, V. R. Stamenkovic, X. Zuo, M. Balasubramanian, V. B. Prakapenka, C. S. Johnson, T. Rajh, *ACS Nano*, 2012, **6**, 530.
24 Q. Liu, Z. Li, Y. Liu, H. Zhang, Y. Ren, C. Sun, W. Lu, Y. Zhou, L. Stanciu, E. A. Stach, J. Xie. *Nat. Comm.*, 2015, **6**, 6127.
25 F. Feng, S. Hu, Y. Guo, J. Zhao, N. Y. Chan, L. Fei, W. Yan, W. Ning, J. Yang, Y. Wang, Y. Xie, C. Wu, *Chem. Commun.*, 2013, **49**, 10462.
26 I. Djerdj, A. M. Tonejc *J. Alloy Compd.*, 2006, **413**, 159.
27 T. Ohsaka, F. Izumi, Y. Fujiki, *J. Raman Spectrosc.*, 1978, **7**, 321.
28 F Tian, Y Zhang, J Zhang, C Pan, *J. Phys. Chem. C.*, 2012, **116**, 7515.
29 F. D. Hardcastlet, I. E. Wachs, *J. Phys. Chem.*, 1991, **95**, 5031.
30 S. Lee, H. M. Cheong, M. J. Seong, P. Liu, C. E. Tracy, A. Mascarenhas, J. R. Pitts, S. K. Deb, *J. Appl. Phys.*, 2002, **92**, 1893.
31 H. Igarashi, K. Tsuji, T. Okuhara, M. Misono, *J. Phys. Chem.*, 1993, **97**, 7065.
32 T.P. Moser, Schrader G.L., *J. Catal.*, 1987, **104**, 99.
33 S. O. Saied, J. L. Sullivan, T. Choudhury, C. G. Pearce, *Vacuum*, 1988, **38**, 917.
34 D. Gonbeau, C. Guimon, G. Pfister-Guillouzo, *Surf. Sci.*, 1991, **254**, 81.
35 X. Zhang, H. Li, X. Cui, Y. Lin. *J. Mater. Chem.*, 2010, **20**, 2801.
36 I. E. Rauda, V. Augustyn, L. C. Saldarriaga-Lopez, X. Chen, L. T. Schelhas, G. W. Rubloff, B. Dunn and S. H. Tolbert, *Adv. Funct. Mater.*, 2014, **24**, 6717-6728.
37 Q. Wei, J. Liu, W. Feng, J. Sheng, X. Tian, L. He, Q. An and L. Mai, *J. Mater. Chem. A*, 2015, **3**, 8070-8075.
38 D. V. A. Van, J. Bhattacharya, A. A. Belak, *Acc. Chem. Res.*, 2013, **46**, 1216.
39 A. Meitav, E. Peled, *J. Electrochem. Soc.*, 1981, **128**, 825.
40 Y. Shunsuke, I. Tetsu, S. Yoshimasa, Y. Shingo, D. Takayuki, M, Kuniaki, M. Eiichiro, *J. Mater. Chem. A*, 2013, **2**, 1144.
41 T. Ichitsubo, S. Okamoto, T. Kawaguchi, Y. Kumagai, F. Oba, S. Yagi, N. Goto, T. Doid, E. Matsubara. *J. Mater. Chem. A*, 2015, **3**, 10188.
42 N. Wu, Z. Yang, H. Yao, Y. Yin, L. Gu, Y. Guo. *Angew. Chem. Int. Ed.*, 2015, **54**, 5757.
43 X. Wang, C. Niu, J. Meng, P. Hu, X. Xu, X. Wei, L. Zhou, K. Zhao, W. Luo, M. Yan, L. Mai. *Adv. Energy Mater.* 2015, **5**, 1500716.
44 M. Wang, M. Yang, L. Ma, X. Shen, X. Zhang. *J. Nanomater.*, 2014, **2014**, 4.
45 R. P. Netterfield, P. J. Martin, C. G. Pacey, W. G. Sainty, D. R. McKenzie, G. J. Auchterlonie, *Appl. Phys.*, 1989, **66**, 1805.
46 D. Gonbeau, C. Guimon, G. Pfister-Guillouzo, A. Levasseur, G. Meunier, R. Dormoy, *Surf. Sci.*, 1991, **254**, 81.
47 C. Sleigh, A. P. Pijpers, A. Jaspers, B. Coussens, R. J. Meier, *J. Electron Spectrosc. Relat. Phenom.* 1996, **77**, 41.
48 P. Moreau, G. Ouvrard, P. Gressier, P. Ganal, J. Rouxel, *J. Phys. Chem. Solids*, 1996, **57**, 1117.
49 R.J. Colton, A.M. Guzman, J.W. Rabalais, *J. Appl. Phys.*, 1978, **49**, 409.
50 R. Gopalakrishnan, B.V.R. Chowdari, K.L. Tan, *Solid State Ionics*, 1992, **53**, 1168.
51 C. Jae-Hyun, M. Aykol, S. Kim, H. Jung-Hoon, C. Wolverton, K. Y. Chung, K. Kwang-Bum, Cho. Byung-Won, *J. Am. Chem. Soc.*, 2014, **136**, 16116.
52 Y. Cheng, Y. Shao, J. Zhang, V. L. Sprenkle, J. Liu, G. Li. *Chem. Commun.*, 2014, **50**, 9644.
53 C. Hsu, C. Chou, C. Yang, T. Lee, J. Chang. *Chem. Commun.*, 2016, **52**, 1701.
54 W. Pan, X. Liu, X. Miao, J. Yang, J. Wang, Y. Nuli, S. Hirano. *J. Solid State Electrochem.*, 2015, **19**, 3347.
55 Y. Yao, L. Zhang, X. Bie, H. Chen, C. Wang, F. Du, G. Chen., *Chem. Eur. J.*, 2017, **23**, 17935.